Chemosphere 251 (2020) 126074

Contents lists available at ScienceDirect

Chemosphere

journal homepage: www.elsevier.com/locate/chemosphere

Adsorption of Polycyclic Aromatic Hydrocarbons from aqueous solution by Organic Montmorillonite Sodium Alginate Nanocomposites

Wen-Jing Dai [a, c], Pan Wu [a], Di Liu [d], Jian Hu [b, *], Yang Cao [e], Tao-Ze Liu [c], Chukwunonso Peter Okoli [f], Bing Wang [a], Ling Li [c]

[a] College of Resource and Environmental Engineering, Guizhou University, Guiyang, 550025, PR China
[b] Research Center for Eco-Environmental Sciences, Chinese Academy of Sciences, Beijing, 100085, PR China
[c] State Key Laboratory of Environment Geochemistry, Institute of Geochemistry, Chinese Academy of Sciences, Guiyang, 550002, PR China
[d] Institute of Atmospheric Physics, Chinese Academy of Sciences, Beijing, 100029, PR China
[e] School of Chemistry and Chemical Engineering, Guizhou University, Guiyang, 550025, PR China
[f] Department of Chemistry/Biochemistry, Alex Ekwueme Federal University Ndufu Alike, Ebonyi State, Nigeria

HIGHLIGHTS

- A high biocompatibility, mechanical stability and adsorption efficiency adsorbent was synthesized for the removal of PAHs in aqueous medium.
- Adsorption mechanism was discussed preliminary.
- It provided a new idea for developing novel and efficient adsorbents.

ARTICLE INFO

Article history:
Received 23 September 2019
Received in revised form
23 January 2020
Accepted 29 January 2020
Available online 12 February 2020

Handling editor: Derek Muir

Keywords:
PAHs
Organic clay
Sodium alginate
Adsorption

ABSTRACT

The adsorption method is generally considered a promising technique to remove inorganic and organic contaminants in an economically and environmentally friendly superior manner. In this study, organic montmorillonite sodium alginate composites were prepared, in which, montmorillonite and cationic surfactant (cetyltrimethylammonium bromide, CTAB) in different added amounts were coagulated with sodium alginate using $CaCl_2$ as the crosslinking agent. The morphological properties of the composites were characterized thoroughly and employed in three typical target pollutants of polycyclic aromatic hydrocarbons (PAHs) (acenaphthene, fluorene, and phenanthrene) by batch adsorption experiments from aqueous solution. The composites provide an efficient alternative for PAHs removals. The composites could be stably separated and regenerated with methyl alcohol. Furthermore, the adsorption kinetic and isotherm data were well described by the Elovich kinetic and the Freundlich isotherm model, respectively. According to these, the adsorption process occurred via multilayer adsorption on the composite's energetically heterogeneous surface. Moreover, pore diffusion and hydrophobicity played a dominant role in the adsorption mechanism. Overall, our study offers a developed adsorbent that has the advantage of being recyclable, low cost, biodegradable and biocompatible for effectively removing PAHs from aqueous solution.

1. Introduction

Organic pollutants, such as polycyclic aromatic hydrocarbons (PAHs) are being continuously released into the available water resource for human consumption via natural and anthropogenic pathways such as from incomplete combustion of fossil fuel, oil spills, and wastewater discharge from the petrochemical industry (Johnsen et al., 2005; Núñez-Delgado et al., 2018; Muangchinda et al., 2018; Mojiri et al., 2019; Wang et al., 2019b). PAHs are persistent organic pollutants that are characterized by chemical stability and highly resistant to biodegradation are widespread

* Corresponding author. Research Center for Eco-Environmental Sciences, Chinese Academy of Sciences No. 18 Shuangqing Road, Beijing, 100085, PR China.
E-mail address: jianhu@rcees.ac.cn (J. Hu).

https://doi.org/10.1016/j.chemosphere.2020.126074
0045-6535/

occurrence of hydrophobic compounds in the environment (Gaur et al., 2018). As a result, several of PAHs have been associated with lung, bladder, stomach and skin cancer (Siddens et al., 2012; Xu et al., 2013). Furthermore, recent studies have indicated that the risk of gene mutations is increased owing to excessive exposure to PAHs (Gaur et al., 2018; Chiang et al., 2009; Delgado-Saborit et al., 2011; Goswami et al., 2018). Hence, due to their carcinogenic and mutagenic effects, developing appropriate methods to treat PAHs from contaminated water has attracted extensive attention (Rubio-Clemente et al., 2014).

The abatement of PAHs pollution in the environment has long been one of the hot issues in scientific research and the main methods include adsorption (Balati et al., 2015; Chomanee et al., 2018), chemical oxidation (Usman et al., 2016; Davin et al., 2018; Boulange et al., 2019), and bioremediation. (Bhatnagar and Sillanpää, 2010; Megharaj et al., 2011; Peng et al., 2014; Anna et al., 2018). Considering its operational simplicity, the nonexistence of secondary by-products and the low cost for maintenance and investment, the adsorption method is a relatively economic and environmental friendly option for aqueous PAH pollution control (Lamichhane et al., 2016; Wang et al., 2019c). Our literature survey showed that there has been considerable effort to develop efficient and cheap adsorbents for PAHs removals (Chen et al., 2015). Many studies have been carried out on the preparation of adsorbents that have stable structure, easy recovery, and high efficiency for PAHs adsorption (Wang et al., 2014; González-Santamaría et al., 2018). Thus far, clay minerals (Kong et al., 2011; Ugochukwu and Fialips, 2017; Safari et al., 2019), carbonaceous materials like biochar (Zhang et al., 2013; Gupta, 2015; Yang et al., 2016), cross-linked starch (Okoli et al., 2014, 2015), carbon nanotubes, and mesoporous materials (Grassi et al., 2012; Costa et al., 2017). have been explored for removal.

Among the studied adsorbents, clay minerals have considerable potential as PAHs adsorbents (Vidal et al., 2011; Zhang et al., 2015; Sabah and Ouki, 2017). They have as strong water absorption capacity, large specific surface area, low cost, and many sources. Among the various naturally abundant clay types, bentonite has been widely used for the removal of PAHs from wastewater because of its high mechanical stability and cost effectiveness (Anirudhan and Ramachandran, 2015). Bentonite is composed of montmorillonite (MMT), and the crystal structure contains abundant exchangeable inorganic cations and H_2O molecules. Hence, MMT is essentially hydrophilic and has little affinity for hydrophobic organic pollutants. To provide the surfaces of clay minerals with hydrophilicity, the clay's interlayer exchangeable inorganic cations have been replaced by the desired organic cations via ion-exchange reactions (Ugochukwu and Fialips, 2017). The results indicated that organic clays synthesized from long-chain hydrocarbons and short-chain hydrocarbons can effectively remove organic compounds effectively. Long-chain quaternary ammonium salt of organic cations can replace exchangeable cations and H_2O molecules in the interlayer domain of MMT and enhance the hydrophobicity (Zhao et al., 2015; Yang et al., 2017). Owing to the strong van der Waals interaction of long-chain alkanes in the interlayer domain, the interference of H_2O molecules is reduced, and the increase in interlayer spacing promotes the distribution of solutes to the organic phase, which has certain advantages in for the removal of PAHs (Karaca et al., 2016).

However, the particle size of MMT as modified by long-chain quaternary ammonium salt organic compounds is relatively small, which makes it unsuitable for largescale wastewater treatment, because the adsorbents usually form a nano-based colloidal suspension. This situation results in the formation of an industrial sludge from the adsorption reactor, which constitute secondary pollution, and increases the separation cost due to difficulty in separating the nano-based colloidal suspension from the water media. Therefore, it is desirable to granulate and encapsulate the nanoparticles in a polymeric scaffold so that the prepared material can be easily separated after adsorption because this enhancement can improve the reusability. (Afzal et al., 2018; Kang et al., 2018; Thakur et al., 2018). In this regard, organic montmorillonite and biomaterials have been developed into alginate-based composites to improve the mechanical properties, swelling properties and adsorption capacity of adsorbents (Wang et al., 2018b), which can be used to remove antibiotics (Thakur et al., 2016; Sadri et al., 2018), dyes (Belhouchat et al., 2017; Garmia et al., 2018; Pawar et al., 2018), and other organic pollutants (Shi et al., 2013; Fei et al., 2016). The composites have the advantages of a high adsorption limit, recyclability, and uninterrupted reuse (Smol and Włodarczyk-Makuła, 2016). They can be used for potential environmental protection and are economic and natural biodegradable macromolecule nano-adsorbent materials that have good biocompatibility (Wang et al., 2018a).

In this study, PAHs in aqueous solution were removed by adsorption using organic montmorillonite, and cetyltrimethylammonium bromide (cationic surfactant) was used as modification reagent. The aim of this study was to determine the effectiveness of organic montmorillonite sodium alginate (OM-SA) as a new adsorption material for PAHs removal from aqueous solution. Acenaphthene (Ace), fluorene (Flu), phenanthrene (Phe) were selected as the model target pollutants for this study owing to their environmental relevance. The effects of different pH and temperature conditions on the adsorption efficiency were explored. The adsorption isotherm model, adsorption kinetics and thermodynamic parameters were determined, and the adsorption mechanism was also explored.

2. Materials and methods

2.1. Chemicals and materials

Montmorillonite-K10 (MMT, GR), chitosan (90%+, deacetylated, GR), alginic acid sodium salt (SA, GR, viscosity of 200–500 Pa s), cetyltrimethylammonium bromide ($C_{19}H_{42}BrN$, 99%, GR), acetonitrile and methyl alcohol (HPLC-grade solvent) were obtained from Shanghai Titan Scientific Co., Ltd (Shanghai, China). Ace (99.6%, Dr. Ehrenstorfer GmbH, Germany), Flu (99%, Dr. Ehrenstorfer GmbH, Germany), and Phe (99%, Dr. Ehrenstorfer GmbH, Germany) were purchased from Anpel Laboratory Technologies (Shanghai) Inc. (Shanghai, China) and used as received without further purification. The relevant properties of the PAHs are shown in Table A1. All other reagents used were of analytical grade. All solutions were prepared using Milli-Q water.

2.2. Preparation of organic montmorillonite

Organic montmorillonite was prepared by adding CTAB (a cationic surfactant) that contains a long alkane chain. The weight ratio between CTAB and MMT were 1:50, 2.5:50, 3:50, and 5:50 which was referred to OM 0.02, OM 0.05 , OM 0.06, OM 0.1, respectively. CTAB was dispersed in 200 mL of Milli-Q water and purified MMT was added in the solution separately to the achieve the same volume (500 mL). The mixed solution was stirred for 3 h at 60 rpm min^{-1} at the 60 °C. The solid and aqueous phases were separated by centrifuge at 3500 rpm min^{-1} for 5 min and dried in a muffle furnace (box) at 105 °C for 12 h.

2.3. Organic montmorillonite composites/montmorillonite composite beads

Powder MMT, OM 0.02, OM 0.05, OM 0.06, and OM 0.1 were encapsulated into composite beads using SA and $CaCl_2$ as the crosslinking agent (Belhouchat et al., 2017). SA (2% (w/v)) was stirred at 60 rpm and 60 °C for 30 min for water bath heating. Then, 5.000 g of powder MMT, OM 0.02, OM 0.05, OM 0.06, and OM 0.1 was added to 100 mL of Milli-Q water. The SA and OM solutions were mixed and stirred (60 rpm) at room temperature for 3 h. The slurry was dropped into composites solution containing 200 mL of 3% (w/v) $CaCl_2$ using a dropper to form beads. After 3–4 d, the composite beads were washed with Milli-Q water 3–5 times and dried in the oven for 48 h at 40 °C, and they will be referred to as MMT-SA, OM 0.02-SA, OM 0.05-SA, OM 0.06-SA, and OM 0.1-SA composites respectively.

2.4. Characterization of the adsorbents

The characterization of the composites, MMT, OM, SA and chitosan was performed using scanning electron microscopy (SEM), X-ray diffraction (XRD), fourier transform infrared spectroscopy (FT-IR) and nitrogen adsorption. The surface morphology of the composites was observed via SEM at 15 kV and 25 kV (JSM-6460LV, Japan) with 50–100 magnification. The XRD pattern was recorded using an X-ray diffractometer (Shimadzu/XRD-6100, Japan), operating at 40 kV and 30 mA with Cu-Kα radiation (λ = 0.15405 nm), a scan range of 5°–80°, and a scan speed of 5.0000 deg min^{-1}. The surface of the functional groups of the composites was determined via FT-IR (Nicolet 380, America) in the range of 400–4000 cm^{-1}. BET surface area and pore size distribution were measured by nitrogen adsorption using the instrument from America (Gemini VII 2390). Nitrogen sorption isotherm of samples was measured at −196 °C and degassed at 150 °C, related pressure (p/p^0) of 0.01–0.999.

2.5. Adsorption experiments

Of the synthesized composites, the OM 0.06-SA composite was used to perform the adsorption experiments. PAHs adsorption experiments were performed using a batch method. Owing to the low solubility of PAHs in water, a solid PAH (Ace, Flu, and Phe) standard was formulated with pure acetonitrile to make a standard stock solution that was 1000 mg L^{-1}. The concentration of acetonitrile was 10% (v/v) in the synthetic wastewater. The solid-to-solution ratio was set at 1:100 with 0.2000 g of adsorbent and 20 mL PAH solution in 40 mL brown glass bottles with polytetrafluoroethylene lined screw caps that were agitated in the dark at 200 rpm and at 25 ± 1 °C. The effect of solution pH (2, 3, 4, 5, 6, and 7) and the temperature (25, 35, 45 °C) on the adsorption of the PAHs was investigated. The initial PAH concentrations ranged from 1 to 9 mg L^{-1} with an initial pH of 5–6 according to the isotherm adsorption. Adsorption kinetic experiments were carried out using an initial concentration of 2 mg L^{-1} PAHs (Ace, Flu, and Phe). The possible loss of PAHs to the glass walls of the adsorption reactor was assessed by measuring the concentration of PAHs in the sample without the adsorbent control group, and the result confirmed that the loss was negligible. The pH of the solution was adjusted by the HCl and NaOH (1 M). After equilibrium was attained, 3–4 mL of the sample was filtered using a disposable glass fiber filter (0.45 μm, 13 mm in diameter) and then analyzed for PAH concentration by high performance liquid chromatography (Agilent 1260 Infinity, USA). Calibration curves involved six test concentrations and correlation coefficients (R^2) over 0.999. Based on the calibration curves, the final concentrations of the samples were calculated. The amounts and removal efficiency (R%) of the adsorbed PAHs adsorbed were derived from initial and final concentrations and calculated using the following equations (Eqns (1)–(3)) :

$$Q_e = \frac{(C_0 - C_e) \times V}{m} \quad (1)$$

$$Q_t = \frac{(C_0 - C_t) \times V}{m} \quad (2)$$

$$R\% = \frac{(C_0 - C_e)}{C_0} \times 100 \quad (3)$$

where C_0 (mg L^{-1}) and C_e (mg L^{-1}) are the initial and equilibrium (final) liquid-phase concentration of PAHs, C_t (mg L^{-1}) is the concentration at t (time), V(L) is the working volume of the solution, and m (g) is the adsorbent mass.

2.6. Desorption experiments

To test the stability and regeneration ability of the prepared composites during wastewater treatment, the prepared OM 0.06-SA composite was used for four adsorption-desorption cycles to determine its reusability (Shahbazi et al., 2011). Experiments were carried out with the adsorbent concentration at 10 g L^{-1} (0.200 g of the adsorbent into 20 mL of PAH solution; Ace, Flu and Phe with concentration of 5, 5, and 6 mg L^{-1}, respectively) in 60 mL brown glass bottles at 200 rpm, 25 ± 1 °C, and at a pH of 6.5 for 24 h. PAHs loaded on OM 0.06-SA were desorbed in 50 mL of methanol and stirred for 4 h (Balati et al., 2015).

3. Results and discussion

3.1. Characterization of the adsorbents

The surface morphologies of the SA and OM-SA composite are shown in Fig. A.1. The SEM image suggests that the SA particles had a porous structure Fig. A.1a. The composite was spherical Fig. A.1, and a large number of protrusions on the surface caused an uneven, rough, and fissured surface Fig. A.1c, and the internal images showed a tight ridge-like structure (Fig. A.1d), indicating that the SA molecules and organic montmorillonite formed a porous three dimensional internal structure of that was chemically cross-linked (Lalhmunsiama et al., 2017).

The FT-IR spectra of the OM composites, SA, chitosan, CTAB, and MMT are shown in Fig. 1. The strong bands of 2971 and 2848 cm^{-1} were assigned to the symmetric and antisymmetric stretching vibrations of the methylene group (−CH_2−), as shown in Fig. 1a. The broad peak at 3390 cm^{-1} for chitosan (Fig. 1b) is attributed to multiple absorption peaks of −OH and −NH stretching vibration. The peak at 3399 cm^{-1} for CTAB (Fig. 1c) is attributed to the −OH stretching vibration and the absorption bands at 1618 and 1418 cm^{-1} were assigned to the symmetric and antisymmetric stretching vibrations of COO−. In Fig. 1d, the broad band at 3624 cm^{-1} is the −OH stretching mode related to octahedral (Si, Al) −OH−Al cations, and 3420 cm^{-1} is ascribed to the −OH stretching band for interlayer water of MMT. The strong band observed at 1037 cm^{-1} is due to Si−O−Si stretching vibration for layered silicates and Si−O bending vibrations were observed at 520 and 450 cm^{-1}.

The XRD patterns of MMT, OM 0.01, OM 0.1, and the OM 0.1-SA composite are shown in Fig. 2. The d_{001} value of MMT changed from 15.225 Å to 16.000 Å ($2\Theta = 5.80°–5.52°$), which indicated that the interlayer spacing of MMT increased after the formation of the composites. This may have been due to the high concentration of SA

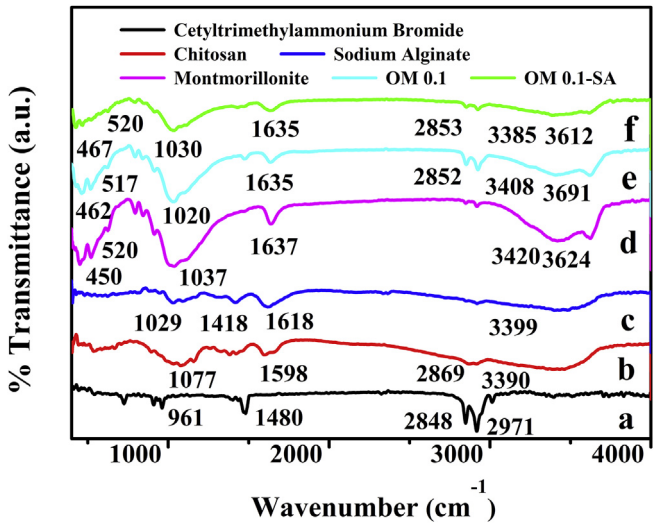

Fig. 1. FTIR spectra of the samples: (a) cetyltrimethylammonium bromide (CTAB); (b) chitosan; (c) sodium alginate (SA); (d) montmorillonite (MMT); (e) organic montmorillonite 0.1 (OM 0.1) (f) organic montmorillonite 0.1− sodium alginate composite (OM 0.1-SA).

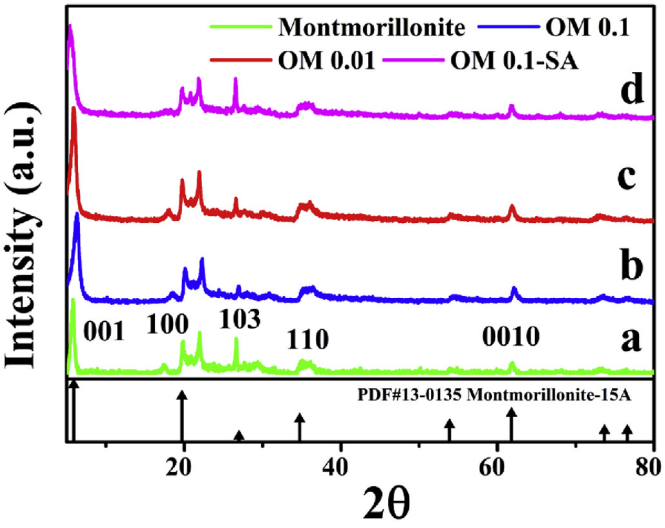

Fig. 2. XRD analysis of MMT (a), OM 0.01 (b), OM 0.1 (c) and the OM 0.1-SA composite (d).

and CTAB molecules inserted into the interlayer structure of MMT.

Fig. A.2 shows the N_2 adsorption−desorption isotherms of the OM 0.02-SA and OM 0.1-SA composites. The N_2 adsorption isotherms of the OM 0.02-SA and OM 0.1-SA composites are similar to a type III isotherm with the characteristic hysteresis loop, and there is an inflection point (B) in the curves. At a low relative pressure ($p/p^0 = 0-0.3$), the amount of N_2 gas by adsorption was relatively lower. With an increasing relative pressure, the intake of N_2 gas increased. The hysteresis loop was considered to be type H3 and indicated that the prepared materials possessed uneven pores. This may have been due to the slit formed by the accumulation of flaky particles. The resulting BET surface area and pore volume of the N_2 adsorption isotherm for the samples are given in Table 1.

3.2. Effect of the surfactant dosage

The removal rate of PAHs by the adsorbents with different amounts of surfactant added (MMT-SA, OM 0.02-SA, OM 0.06-SA, OM 0.1-SA) at 25 °C in shown in Fig. A.3. The removal efficiencies of the PAHs on the modified adsorbents were over 70%. The adsorption of PAHs on modified MMT was related to the types and concentration of cationic surfactant, and the properties of the PAHs. PAHs are persistent organic pollutants that have a stable chemical structure and hydrophobicity increases to with a the increase in molecular weight, in contrast to solubility (Zhu et al., 1998). The adsorption capacity increased with elevated amount of cationic surfactant, which was ascribed to the increased amount of the surfactant entering the MMT layer, enlarging the interlayer space. This, enhanced the hydrophobicity and organophilic ability.

Table 1
BET surface area and other pore parameters for OM 0.02-SA and OM 0.1-SA.

Parameters	Samples		
	MMT	OM 0.02-SA composite	OM 0.1-SA composite
BET surface area ($m^2\ g^{-1}$)	55.428	22.560	24.436
Total Pore Volume ($cm^3\ g^{-1}$)	——	0.113	0.101
Pore Radius (nm)	——	1.529	3.426
BJH Surface Area ($m^2\ g^{-1}$)	——	22.560	18.971

3.3. Effect of pH on PAH adsorption

The effect of solution pH on the adsorption efficiency of PAHs was studied using OM 0.05-SA as the adsorbent and as shown in Fig. A.4. As the pH increased from 2 to 8, the amount of adsorbed PAH decreased. This decreased adsorption was attributed to the surface charge of the adsorbent, and the degree of ionization, and the morphology of the target contaminants. At low pH, too much H^+ can cause an imbalance in the positive and negative charges on the surface of the adsorbent. In this study, OM 0.05-SA was rich in actively functional groups (Si—OH, —COOH, $-NH_2$), which were protonated at low pH. The protonation of oxygen-containing functional groups enhanced the hydrophobicity of the adsorbent. Therefore, a low pH increased the electrostatic interaction between the surface charges of the adsorbent and PAHs. Although the maximum amount of adsorption occurred at a pH of 2, the initial pH for this experiment was chosen to be 5−6, because a pH in this range was is closer to the pH of the real wastewater.

3.4. Adsorption kinetics

Adsorption kinetics is one of the most significant steps in studying adsorption processes. It reflects the relationship between the contact time and the amounts of PAHs adsorbed (Hamoudi and Belkacemi, 2013; Wang et al., 2019a). For this investigation, the experimental data were analyzed using the following four adsorption kinetic models: PFO, PSO, Elovich, and intra-particle diffusion, as shown in Fig. 3, and the values of correlative parameters are summarized in Table A.2. The results of the kinetics study showed that the adsorption of PAHs on the composites reached equilibrium within 12 h. The PSO and Elovich kinetic models fit well to the PAHs, and the calculated equilibrium quantities adsorbed ($Qe_{(cal)}$) were close to the experimental values ($Qe_{(exp)}$), indicating pore mass transfer was involved and chemical adsorption played a significant role in the adsorption process (Kim et al., 2013). At the initial adsorption stage, the concentration gradient constitutes a high adsorption force that can overcome the external mass transfer resistance, and the PAHs molecules can be easily captured due to the high affinity active for the sites on the surface of the composites. As the active sites with lower affinity get filled, the rate of

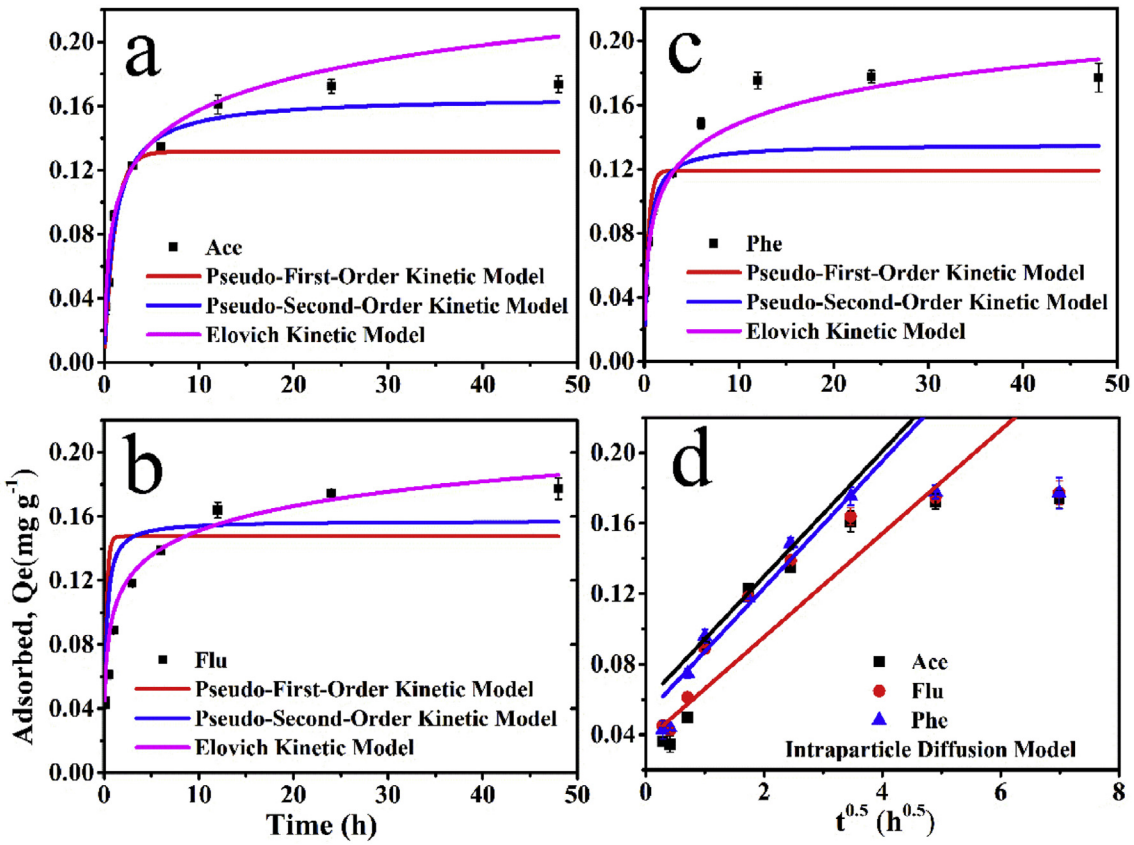

Fig. 3. (a) Kinetic models for Ace, (b) Kinetic models for Flu (c) Kinetic models for Phe, (d)Intraparticle diffusion for the PAH (Ace, Flu, and Phe) adsorption onto OM 0.06-SA. The initial concentration of Ace, Flu, and Phe in each case was 2 mg L^{-1} adsorbent dose of 0.200 g, the solution volume of 0.02 L, pH 5–6.

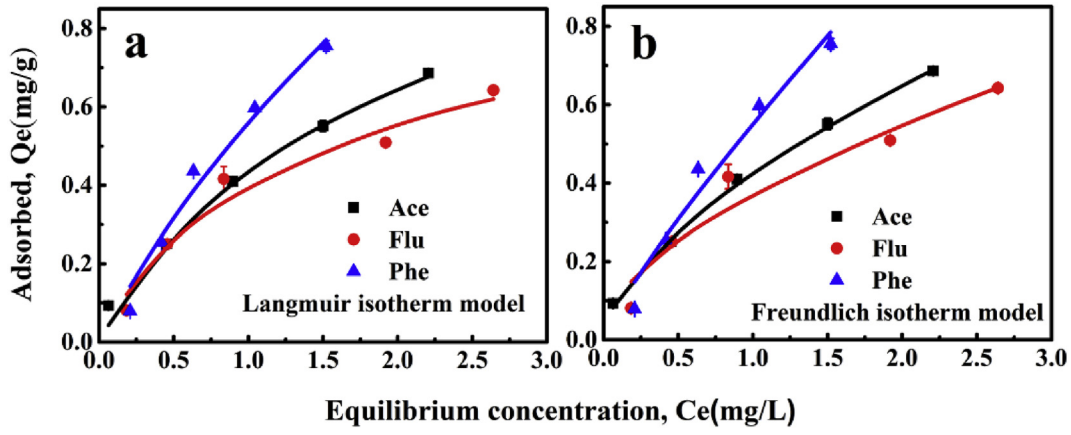

Fig. 4. (a) Langmuir and (b) Freundlich isotherm models: the adsorption of PAHs (Ace, Flu, and Phe) onto OM 0.06-SA with initial concentrations of PAHs of 1, 3, 5, 7, and 9 mg L^{-1}, an adsorbent dose of 0.200 g, a solution volume of 0.02 L, and a pH of 5–6.

adsorption changed from fast to slow and finally reach equilibrium.

The mass transfer process between the adsorbate and the adsorbent mainly involves the adsorbate is being adsorbed by the external mass transfer across the boundary layer around the adsorbent, adsorbing on the active sites of the adsorbent through physical or chemical bonds. Through the internal mass transfer (pore wall or holes), the adsorbate entered the interior of the adsorbent. The intraparticle diffusion model can be used to determine the control mechanism of the adsorption process. This study applied the linear form of the intraparticle diffusion model equation (Eqn (4)):

$$Q_t = K_i t^{0.5} + c \quad (4)$$

where k_i (min^{-1}) is the diffusion rate parameter of the intraparticle diffusion model. The fitting of the intraparticle diffusion model is shown in Fig. 3d.

At the beginning of the adsorption, the slope of the curve was high (Fig. 3), indicating that rapid adsorption occurred on the surfaces of the composites. The rate of adsorption slowed until equilibrium was attained after a period of time. During the adsorption process, the rate of the entire process was controlled by the slowest

Table 2
Langmuir adsorption capacities of the adsorption materials compared to those previous studies on PAHs in the literature.

Adsorption materials	PAHs	Adsorbent concentration/g L^{-1}	Surface area/ m^2 g^{-1}	Adsorption capacity/ mg g^{-1}	Reference
Orange rind activated carbon	Phenanthrene	0.25	352	70.92	Gupta (2015)
Modified palm shell activated carbon by KOH	Acenaphthene	4.00	286	96.54	Kumar et al. (2019)
Silica-based organic inorganic nanohybrid	Naphthalene	3.00	–	1.92	Balati et al. (2015)
	Acenaphthylene			1.41	
	Phenanthrene			0.76	
Mesoporous molecular sieve	benzo [b]fluoranthene benzo	10.00	1166	0.15	Costa et al. (2017)
	[k]fluoranthene benzo [a]pyrene			0.15	
				0.16	
Modified montmorillonite by L-carnitine and choline	Benzo [a] pyrene	1.00	–	0.09	Wang et al. (2019c)
				0.09	
Sepiolite	Pyrene	0.50	358	8.10	Sabah and Ouki (2017)
Modified montmorillonite by CTBA	Acenaphthene	10.00	24	1.20	This study
	Fluorene			0.90	
	Phenanthrene			2.50	

steps (boundary layer diffusion and particle diffusion). As shown in Fig. 3d, the plots of Q_t and $t^{0.5}$ are linear, but not pass through the origin, indicating that intraparticle diffusion was not the only rate-limiting step, and other mechanisms are involved (Sun et al., 2015). The intercept provides an estimate of the thickness of the boundary layer. The larger the value of the intercept, the greater the effect of the boundary layer.

3.5. Adsorption isotherms

Adsorption isotherms describe the interaction and behavior between an adsorbent and adsorbate (Ueda Yamaguchi et al., 2016). The fitting of Langmuir and Freundlich adsorption isotherm models was applied for the isotherm data, as shown in Fig. 4, and the isotherm parameters are summarized in Table A.3. The Freundlich model fitted better to the PAHs adsorption equilibrium data across the chosen concentration range compared to the Langmuir model. This indicated that the adsorption process involved multilayer adsorption on the nanocomposite's heterogeneous surface. This is consistent with the kinetic study of the adsorption of PAHs on the composites by heterogeneous processes. The active adsorption sites of the composites on the surface were nonuniform and had different affinities for adsorption. This may be due to the nonuniform functional groups at different locations on the surface of the composites. The adsorption capacity for PAHs on the composites was ordered as follows: Phe > Ace > Flu. This is in agreement with the degree of hydrophobicity (K_{ow}), which was Phe > Ace > Flu (Table A.1). Phe exhibited more adsorption on the composites than Ace and Flu, showing that Phe had stronger affinity to the surface of the composites that had more active adsorption sites.

Although adsorption capacity is not generally accepted as reliable indicator for assessing adsorption performance owing to its dependence on the adsorption conditions such as the adsorbate concentration and adsorbent dose, comparison of the adsorption capacity from our current study to the values from literature (Table 2) showed that the developed adsorbent exhibited acceptable performance. Using phenanthrene for as an example, the composite adsorbent exhibited the second-best performance after orange rind activated carbon, despite the fact that mesoporous materials and biochar have large surface areas. Besides exhibiting acceptable adsorption performance, the modified MMT prepared in this study has good biocompatibility and reusability, and the preparation process is relatively simple and cost-effective.

3.6. Thermodynamics study

Temperature is a significant factor in the adsorption process. The tendency of change with temperature and the adsorption thermodynamics of PAHs on the composites are shown in Figs. A.5 and A.6, respectively, and the thermodynamics parameters are summarized in Table A.4. The value of $\triangle H^0$ and $\triangle S^0$ can be obtained from the slope and intercept, respectively, from the plot of $\ln K_d$ against 1/T (Fig. A.6). The calculated values of $\triangle G^0$ were negative, which indicated that the PAHs adsorption on the composites was spontaneous. The positive value of enthalpy change ($\triangle H^0$) indicated the adsorption process is endothermic in nature as, the removal rate of PAHs increased with temperature. Meanwhile, $\triangle S^0 > 0$ reflected the increased randomness at the solid–solution interface during the adsorption process.

3.7. Desorption

The desorption capacity of OM 0.06-SA and the results of the adsorption-desorption cycle experiments are shown in Fig. 5. Using phenanthrene for example, after four adsorption–desorption cycles, the adsorption performance of the composite indicated losses of 31.71%, 39.56%, and 59.45% in terms of the adsorption capacity, for the second, third, and fourth cycles, respectively, compared to the initial (first) cycle. This observation indicated that OM 0.06-SA has a good reusability and stability, and thus, may be appropriate for the removal of PAHs in practical applications.

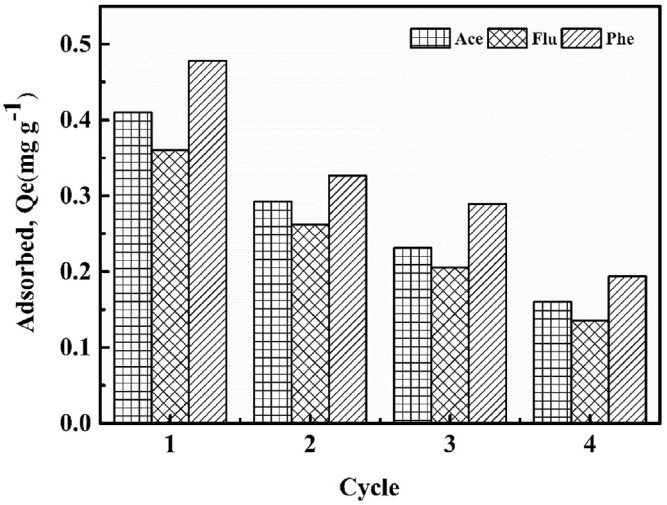

Fig. 5. Adsorption–desorption cycles of PAHs (Ace, Flu, and Phe) onto OM 0.06-SA. The initial concentrations of PAHs were 5, 5, and 6 mg L^{-1}, respectively, with an adsorbent dose of 0.200 g, a solution volume of 0.02 L, and a pH of 5–6.

4. Conclusions

Our results showed that the OM composites were effective for PAH removal. The Freundlich isotherm model and the Elovich kinetic model fit the experimental data. Pore diffusion and hydrophobicity played a dominant role in the adsorption mechanism. The interaction between the PAHs and the composites was hydrophobic in nature which was driven by wan der Waals forces. In addition, the composite adsorbents had the advantage of being low cost and biodegradable, and good biocompatibility. Hence, they could be efficiently used for wastewater treatment to prevent PAH pollution.

CRediT authorship contribution statement

Wen-Jing Dai: Data curation, Investigation, Writing - original draft. **Pan Wu:** Conceptualization, Validation, Supervision. **Di Liu:** Writing - review & editing, Visualization, Investigation. **Jian Hu:** Methodology, Validation, Resources. **Yang Cao:** Writing - review & editing. **Tao-Ze Liu:** Conceptualization, Methodology. **Chukwunonso Peter Okoli:** Investigation, Writing - review & editing. **Bing Wang:** Visualization, Writing - review & editing. **Ling Li:** Writing - review & editing.

Acknowledgements

This work was supported by the National Key Research and Development Plan of China (Grant No.2018YFC1800306) and the National Natural Science Foundation of China (Grant No.91644104).

Appendix

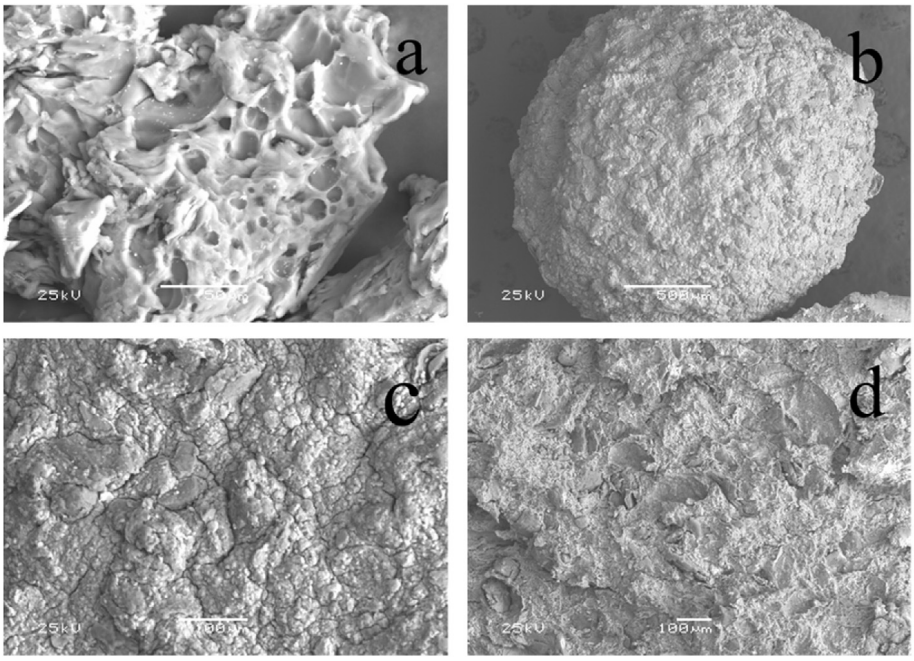

Fig. A.1. SEM images of (a) SA × 500; (b) OM 0.06-SA × 50; (c) OM 0.06-SA × 200; (d) OM 0.06-SA × 100.

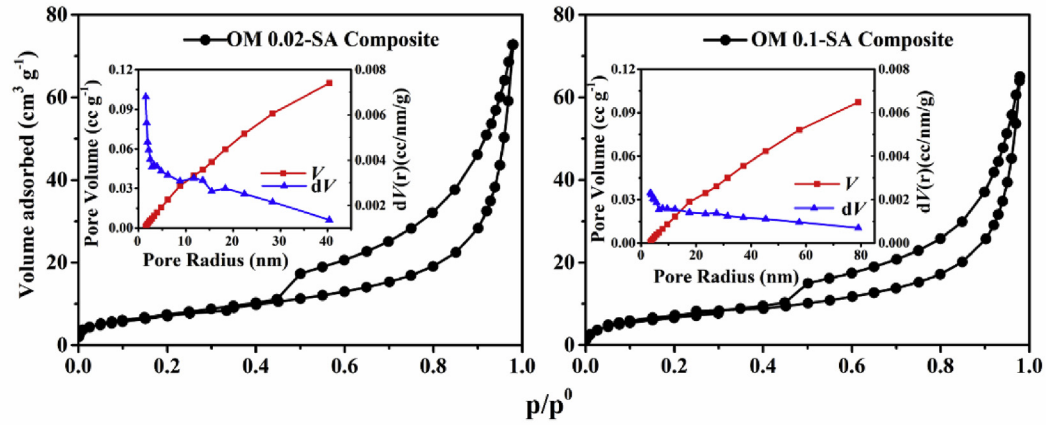

Fig. A.2. N_2 adsorption–desorption isotherms patterns of the OM 0.02-SA and OM 0.1-SA composite.

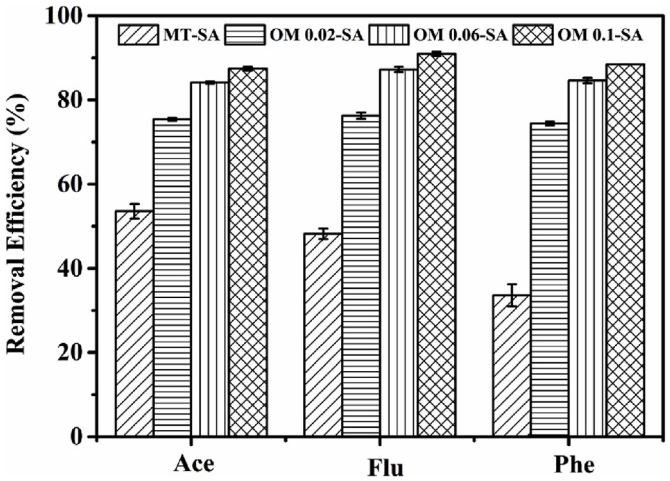

Fig. A.3. Adsorption of PAHs (Ace, Flu, and Phe) on the composites with different amounts of surfactant added with initial concentrations of Ace, Flu, and Phe 2 mg L^{-1}, an adsorbent dose of 0.200 g, and a solution volume of 0.02 L, and a pH of 5–6.

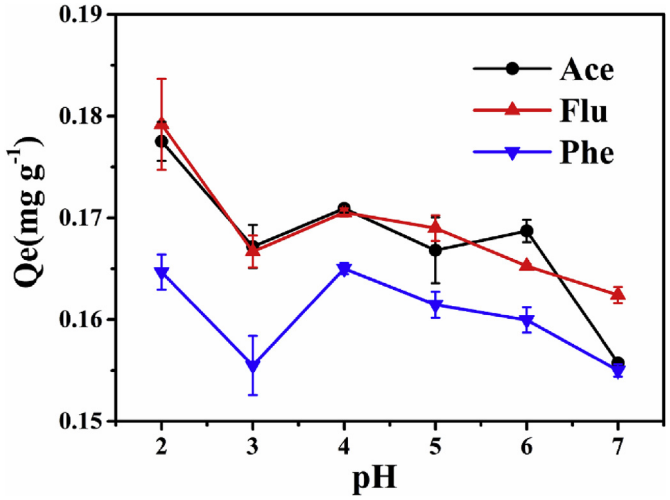

Fig. A.4. Adsorption of PAHs (Ace, Flu, and Phe) on the composites at different pH values (2–8) with initial concentrations of Ace, Flu, and Phe of 2 mg L^{-1} in each case, adsorbent dose of 0.200 g, and a solution volume of 0.02 L.

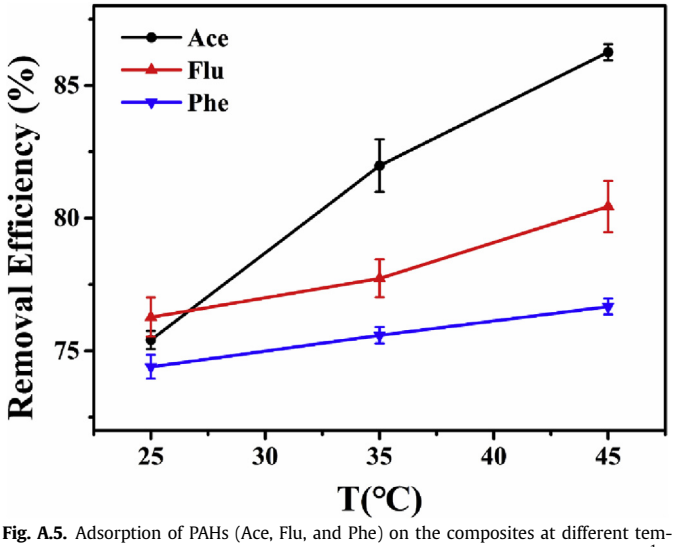

Fig. A.5. Adsorption of PAHs (Ace, Flu, and Phe) on the composites at different temperatures (25, 35, 45 °C) with initial concentration of Ace, Flu, and Phe of 2 mg L^{-1}in each case, an adsorbent dose of 0.200 g, and solution volume of 0.02 L.

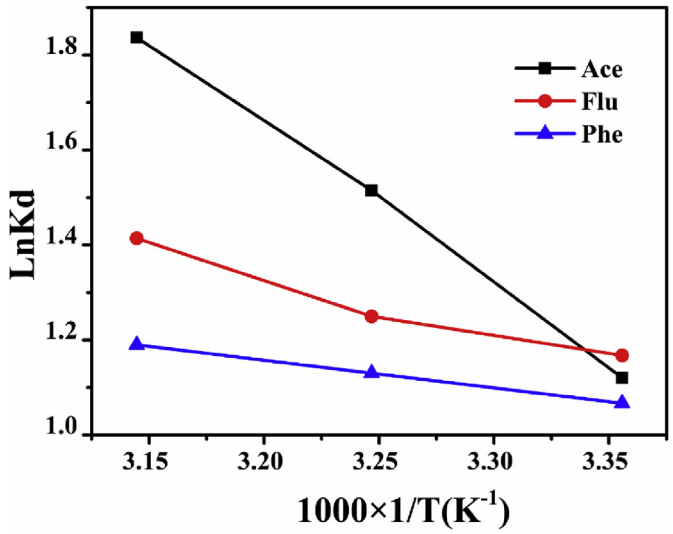

Fig. A.6. Plot of lnK_d vs. 1/T for adsorption of PAHs (Ace, Flu, and Phe) onto OM 0.02-SA.

Table A.1
Structural and physicochemical properties of the PAHs (Smol and Włodarczyk-Makuła, 2016)

PAHs	Structural formula	Molecular weight (g mol^{-1})	Solubility (ng L^{-1}) (in water at 25 °C)	Log (K_{OW})[a]
Acenaphthen (Ace)		154.200	3.900×10^6	4.330
Fluorene (Fln)		166.200	1.980×10^6	4.180
Phenanthrene (Phe)		178.200	1.290×10^6	4.570

[a] N-octanol-water partition coefficient.

Table A.2
Adsorption kinetic parameters obtained for the PAHs using OM 0.06-SA

Kinetic model	Parameters	PAHs		
		Ace	Flu	Phe
Pseudo-first-order	k_1 (h^{-1})	0.776	0.778	1.438
	Qe (mg g^{-1})	0.154	0.163	0.155
	R^2	0.856	0.888	0.755
Pseudo-second-order	k_2 (h^{-1})	3.099	2.842	4.719
	Qe (mg g^{-1})	0.178	0.189	0.178
	R^2	0.907	0.910	0.851
Elovich	A	0.938	0.926	3.118
	B	41.815	39.034	48.683
	R^2	0.969	0.985	0.972
Intraparticle diffusion	Ki (min^{-1})	0.003	0.003	0.002
	C	0.054	0.055	0.073
	R^2	0.834	0.864	0.850

Table. A.3
Isotherm parameters for the adsorption of the PAHs on the composites

Isotherm model	Parameters	PAHs		
		Ace	Flu	Phe
Langmuir	b	0.592	0.849	0.288
	Q_m (mg g^{-1})	1.200	0.900	2.500
	R^2	0.988	0.976	0.968
Freundlich	K_f ($mg^{(n-1)/n}$ g^{-1})	0.430	0.380	0.550
	1/n	0.598	0.551	0.837
	R^2	0.998	0.942	0.966

Table A.4
Thermodynamics parameters of PAHs (Ace, Flu, and Phe) adsorption on the OM 0.06-SA composite.

PAHs	△H (J·mol^{-1})	△S (J $mol^{-1}K^{-1}$)	△G (KJ·mol^{-1})			
			Temperature(K)			R^2
			298	308	318	
Ace	28.24	104.13	−31.00	−32.04	−33.09	0.997
Flu	9.68	42.06	−12.52	−12.94	−13.36	0.915

References

Afzal, M.Z., Sun, X.F., Liu, J., Song, C., Wang, S.G., Javed, A., 2018. Enhancement of ciprofloxacin sorption on chitosan/biochar hydrogel beads. Sci. Total Environ. 639, 560–569. https://doi.org/10.1016/j.scitotenv.2018.05.129.

Anirudhan, T.S., Ramachandran, M., 2015. Adsorptive removal of basic dyes from aqueous solutions by surfactant modified bentonite clay (organoclay): kinetic and competitive adsorption isotherm. Process Saf. Environ. Protect. 95, 215–225. https://doi.org/10.1016/j.psep.2015.03.003.

Anna, K.I., Emanuel, G., Anna, S.R., Blonska, E., Lasota, J., Lagan, S., 2018. Linking the contents of hydrophobic PAHs with the canopy water storage capacity of coniferous trees. Environ. Pollut. 242, 1176–1184. https://doi.org/10.1016/j.envpol.2018.08.015.

Balati, A., Shahbazi, A., Amini, M.M., Hashemi, S.H., 2015. Adsorption of polycyclic aromatic hydrocarbons from wastewater by using silica-based organic–inorganic nanohybrid material. J. Water Reuse Desalin. 5, 50–63. https://doi.org/10.2166/wrd.2014.013.

Belhouchat, N., Zaghouane-Boudiaf, H., Viseras, C., 2017. Removal of anionic and cationic dyes from aqueous solution with activated organo-bentonite/sodium alginate encapsulated beads. Appl. Clay Sci. 135, 9–15. https://doi.org/10.1016/j.clay.2016.08.031.

Bhatnagar, A., Sillanpää, M., 2010. Utilization of agro-industrial and municipal waste materials as potential adsorbents for water treatment—a review. Chem. Eng. J. 157, 277–296. https://doi.org/10.1016/j.cej.2010.01.007.

Boulange, M., Lorgeoux, C., Biache, C., Saada, A., Faure, P., 2019. Fenton-like and potassium permanganate oxidations of PAH-contaminated soils: impact of oxidant doses on PAH and polar PAC (polycyclic aromatic compound) behavior. Chemosphere 224, 437–444. https://doi.org/10.1016/j.chemosphere.2019.02.108.

Chen, F., Hong, M., You, W., Li, C., Yu, Y., 2015. Simultaneous efficient adsorption of Pb^{2+} and MnO_4^- ions by MCM-41 functionalized with amine and nitrilotriacetic acid anhydride. Appl. Clay Sci. 357, 856–865. https://doi.org/10.1016/j.apsusc.2015.09.069.

Chiang, K.C., Chio, C.P., Chiang, Y.H., Liao, C.M., 2009. Assessing hazardous risks of human exposure to temple airborne polycyclic aromatic hydrocarbons. J. Hazard Mater. 166, 676–685. https://doi.org/10.1016/j.jhazmat.2008.11.084.

Chomanee, J., Tekasakul, S., Tekasakul, P., Furuuchi, M., 2018. Effect of irradiation energy and residence time on decomposition efficiency of polycyclic aromatic hydrocarbons (PAHs) from rubber wood combustion emission using soft X-rays. Chemosphere 210, 417–423. https://doi.org/10.1016/j.chemosphere.2018.07.001.

Costa, J.A.S., de Jesus, R.A., da Silva, C.M.P., Romão, L.P.C., 2017. Efficient adsorption of a mixture of polycyclic aromatic hydrocarbons (PAHs) by Si–MCM–41 mesoporous molecular sieve. Powder Technol. 308, 434–441. https://doi.org/10.1016/j.powtec.2016.12.035.

Davin, M., Starren, A., Deleu, M., Lognay, G., Colinet, G., Fauconnier, M.L., 2018. Could saponins be used to enhance bioremediation of polycyclic aromatic hydrocarbons in aged-contaminated soils? Chemosphere 194, 414–421. https://doi.org/10.1016/j.chemosphere.2017.11.174.

Delgado-Saborit, J.M., Stark, C., Harrison, R.M., 2011. Carcinogenic potential, levels and sources of polycyclic aromatic hydrocarbon mixtures in indoor and outdoor environments and their implications for air quality standards. Environ. Int. 37, 383–392. https://doi.org/10.1016/j.envint.2010.10.011.

Fei, Y., Li, Y., Han, S., Ma, J., 2016. Adsorptive removal of ciprofloxacin by sodium alginate/graphene oxide composite beads from aqueous solution. J. Colloid Interface Sci. 484, 196–204. https://doi.org/10.1016/j.jcis.2016.08.068.

Garmia, D., Zaghouane-Boudiaf, H., Ibbora, C.V., 2018. Preparation and characterization of new low-cost adsorbent beads based on activated bentonite encapsulated with calcium alginate for removal of 2,4-dichlorophenol from aqueous medium. Int. J. Biol. Macromol. 115, 257–265. https://doi.org/10.1016/j.ijbiomac.2018.04.064.

Gaur, N., Narasimhulu, K., PydiSetty, Y., 2018. Recent advances in the bioremediation of persistent organic pollutants and its effect on environment. J. Clean. Prod. 198, 1602–1631. https://doi.org/10.1016/j.jclepro.2018.07.076.

González-Santamaría, D.E., López, E., Ruiz, A., Fernández, R., Ortega, A., Cuevas, J., 2018. Adsorption of phenanthrene by stevensite and sepiolite. Clay Miner. 52, 341–350. https://doi.org/10.1180/claymin.2017.052.3.05.

Goswami, L., Manikandan, N.A., Dolman, B., Pakshirajan, K., Pugazhenthi, G., 2018. Biological treatment of wastewater containing a mixture of polycyclic aromatic hydrocarbons using the oleaginous bacterium *Rhodococcus opacus*. J. Clean. Prod. 196, 1282–1291. https://doi.org/10.1016/j.jclepro.2018.06.070.

Grassi, M., Kaykioglu, G., Belgiorno, V., Lofrano, G., 2012. Emerging compounds removal from wastewater: removal of emerging contaminants from water and wastewater by adsorption process. In: Lofrano, G. (Ed.), Emerging Compounds Removal from Wastewater. SpringerBriefs in Molecular Science. Springer, Dordrecht. https://doi.org/10.1007/978-94-007-3916-1_2.

Gupta, H., 2015. Removal of phenanthrene from water using activated carbon developed from orange rind. Int. J. Sci. Res. Environ. Sci. 3 (7), 248–255. https://doi.org/10.12983/ijsres-2015-p0248-0255.

Hamoudi, S., Belkacemi, K., 2013. Adsorption of nitrate and phosphate ions from aqueous solutions using organically-functionalized silica materials: kinetic modeling. Fuel 110, 107–113. https://doi.org/10.1016/j.fuel.2012.09.066.

Johnsen, A.R., Wick, L.Y., Harms, H., 2005. Principles of microbial PAH-degradation in soil. Environ. Pollut. 133, 71–84. https://doi.org/10.1016/j.envpol.2004.04.015.

Kang, Y.G., Vu, H.C., Le, T.T., Chang, Y.S., 2018. Activation of persulfate by a novel Fe (II)-immobilized chitosan/alginate composite for bisphenol A degradation. Chem. Eng. J. 353, 736–745. https://doi.org/10.1016/j.cej.2018.07.175.

Karaca, G., Baskaya, H.S., Tasdemir, Y., 2016. Removal of polycyclic aromatic hydrocarbons (PAHs) from inorganic clay mineral: Bentonite. Environ. Sci. Pollut. Res. 23, 242–252. https://doi.org/10.1007/s11356-015-5676-z.

Kim, E.J., Lee, C.S., Chang, Y.Y., Chang, Y.S., 2013. Hierarchically structured manganese oxide-coated magnetic nanocomposites for the efficient removal of heavy metal ions from aqueous systems. ACS Appl. Mater. Interfaces 5, 9628–9634. https://doi.org/10.1021/am402615m.

Kong, H., He, J., Gao, Y., Han, J., Zhu, X., 2011. Removal of polycyclic aromatic hydrocarbons from aqueous solution on soybean stalk-based carbon. J. Environ. Qual. 40, 1737–1744. https://dl.sciencesocieties.org/publications/jeq/abstracts/40/6/1737.

Kumar, J.A., Amarnath, D.J., Sathish, S., Jabasingh, S.A., Saravanan, A., Hemavathy, R.V., Anand, K.V., Yaashikaa, P.R., 2019. Enhanced PAHs removal using pyrolysis-assisted potassium hydroxide induced palm shell activated carbon: batch and column investigation. J. Mol. Liq. 279, 77–87. https://doi.org/10.1016/j.molliq.2019.01.121.

Lalhmunsiama, Pawar, R.R., Hong, S.M., Jin, K.J., Lee, S.M., 2017. Iron-oxide modified sericite alginate beads: a sustainable adsorbent for the removal of as (V) and Pb (II) from aqueous solutions. J. Mol. Liq. 240, 497–503. https://doi.org/10.1016/j.molliq.2017.05.086.

Lamichhane, S., Bal Krishna, K.C., Sarukkalige, R., 2016. Polycyclic aromatic hydrocarbons (PAHs) removal by sorption: a review. Chemosphere 148, 336–353. https://doi.org/10.1016/j.chemosphere.2016.01.036.

Megharaj, M., Ramakrishnan, B., Venkateswarlu, K., Sethunathan, N., Naidu, R., 2011. Bioremediation approaches for organic pollutants: a critical perspective. Environ. Int. 37, 1362–1375. https://doi.org/10.1016/j.envint.2011.06.003.

Mojiri, A., Zhou, J.L., Ohashi, A., Ozaki, N., Kindaichi, T., 2019. Comprehensive review of polycyclic aromatic hydrocarbons in water sources, their effects and treatments. Sci. Total Environ. 696, 133971. https://doi.org/10.1016/j.scitotenv.2019.133971.

Muangchinda, C., Rungsihiranrut, A., Prombutara, P., Soonglerdsongpha, S., Pinyakong, O., 2018. 16S metagenomic analysis reveals adaptability of a mixed PAH-degrading consortium isolated from crude oil-contaminated seawater to changing environmental conditions. J. Hazard Mater. 357, 119–127. https://doi.org/10.1016/j.jhazmat.2018.05.062.

Núñez-Delgado, A., Sueiro-Blanco, P., Labandeira, S.S., Torrijos, R.C., 2018. Polycyclic aromatic hydrocarbons concentrations in a waste from fuel oil spill and its mixture with other materials: time-course evolution. J. Clean. Prod. 172, 1910–1917. https://doi.org/10.1016/j.jhazmat.2018.05.062.

Okoli, C.P., Adewuyi, G.O., Zhang, Q., Zhu, G., Wang, C., Guo, Q., 2015. Aqueous scavenging of polycyclic aromatic hydrocarbons using epichlorohydrin, 1,6-hexamethylene diisocyanate and 4,4-methylene diphenyl diisocyanate modified starch: pollution remediation approach. Arab. J. Chem. https://doi.org/10.1016/j.arabjc.2015.06.004.

Okoli, C.P., Guo, Q.J., Adewuyi, G.O., 2014. Application of quantum descriptors for predicting adsorption performance of starch and cyclodextrin adsorbents. Carbohydr. Polym. 101, 40–49. https://doi.org/10.1016/j.carbpol.2013.08.065.

Pawar, R.R., Lalhmunsiama, Gupta, P., Sawant, S.Y., Shahmoradi, B., Lee, S.M., 2018. Porous synthetic hectorite clay-alginate composite beads for effective adsorption of methylene blue dye from aqueous solution. Int. J. Biol. Macromol. 114, 1315–1324. https://doi.org/10.1016/j.ijbiomac.2018.04.008.

Peng, R., Fu, X., Tian, Y., Zhao, W., Zhu, B., Xu, J., Wang, B., Wang, L., Yao, Q., 2014. Metabolic engineering of Arabidopsis for remediation of different polycyclic

aromatic hydrocarbons using a hybrid bacterial dioxygenase complex. Metab. Eng. 26, 100–110. https://doi.org/10.1016/j.ymben.2014.09.005.
Rubio-Clemente, A., Torres-Palma, R.A., Peñuela, G.A., 2014. Removal of polycyclic aromatic hydrocarbons in aqueous environment by chemical treatments: a review. Sci. Total Environ. 478, 201–225. https://doi.org/10.1016/j.scitotenv.2013.12.126.
Sabah, E., Ouki, S., 2017. Adsorption of pyrene from aqueous solutions onto sepiolite. Clay Clay Miner. 65, 14–26. https://link.springer.com/article/10.1346/CCMN.2016.064046.
Sadri, S., Johnson, B.B., Ruyter-Hooley, M., Angove, M.J., 2018. The adsorption of nortriptyline on montmorillonite, kaolinite and gibbsite. Appl. Clay Sci. 165, 64–70. https://doi.org/10.1016/j.clay.2018.08.005.
Safari, S., Alam, M.S., von Gunten, K., Samborsky, S., Alessi, D.S., 2019. Inhibition of naphthalene leaching from municipal carbonaceous waste by a magnetic organophilic clay. J. Hazard Mater. 368, 578–583. https://doi.org/10.1016/j.jhazmat.2019.01.088.
Shahbazi, A., Younesi, H., Badiei, A., 2011. Functionalized SBA-15 mesoporous silica by melamine-based dendrimer aminesfor adsorptive characteristics of Pb(II), Cu(II) and Cd(II)heavy metal ions in batch and fixed bed column. Chem. Eng. J 168 (2), 505–518.
Shi, Y., Xue, Z., Wang, X., Wang, L., Wang, A., 2013. Removal of methylene blue from aqueous solution by sorption on lignocellulose-*g*-poly (acrylic acid)/montmorillonite three-dimensional cross-linked polymeric network hydrogels. Polym. Bull. 70, 1163–1179. https://link.springer.com/article/10.1007/s00289-012-0898-4.
Siddens, L.K., Larkin, A., Krueger, S.K., Bradfield, C.A., Waters, K.M., Tilton, S.C., Pereira, C.B., Lohr, C.V., Arlt, V.M., Phillips, D.H., Williams, D.E., Baird, W.M., 2012. Polycyclic aromatic hydrocarbons as skin carcinogens: comparison of benzo[a]pyrene, dibenzo[def,p]chrysene and three environmental mixtures in the FVB/N mouse. Toxicol. Appl. Pharmacol. 264, 377–386. https://doi.org/10.1016/j.taap.2012.08.014.
Smol, M., Włodarczyk-Makuła, M., 2016. The effectiveness in the removal of PAHs from aqueous solutions in physical and chemical processes: a review. Polycycl. Aromat. Comp. 37, 292–313. https://doi.org/10.1080/10406638.2015.1105828.
Sun, P., Hui, C., Azim Khan, R., Du, J., Zhang, Q., Zhao, Y.H., 2015. Efficient removal of crystal violet using Fe_3O_4-coated biochar: the role of the Fe_3O_4 nanoparticles and modeling study their adsorption behavior. Sci. Rep. 5, 12638.
Thakur, S., Pandey, S., Arotiba, O.A., 2016. Development of a sodium alginate-based organic/inorganic superabsorbent composite hydrogel for adsorption of methylene blue. Carbohydr. Polym. 153, 34–46. https://doi.org/10.1016/j.carbpol.2016.06.104.
Thakur, S., Sharma, B., Verma, A., Chaudhary, J., Tamulevicius, S., Thakur, V.K., 2018. Recent progress in sodium alginate based sustainable hydrogels for environmental applications. J. Clean. Prod. 198, 143–159. https://doi.org/10.1016/j.jclepro.2018.06.259.
Ueda Yamaguchi, N., Bergamasco, R., Hamoudi, S., 2016. Magnetic $MnFe_2O_4$ –graphene hybrid composite for efficient removal of glyphosate from water. Chem. Eng. J. 295, 391–402. https://doi.org/10.1016/j.cej.2016.03.051.
Ugochukwu, U.C., Fialips, C.I., 2017. Removal of crude oil polycyclic aromatic hydrocarbons via organoclay-microbe-oil interactions. Chemosphere 174, 28–38. https://doi.org/10.1016/j.chemosphere.2017.01.080.
Usman, M., Hanna, K., Haderlein, S., 2016. Fenton oxidation to remediate PAHs in contaminated soils: a critical review of major limitations and counter-strategies. Sci. Total Environ. 569–570, 179–190. https://doi.org/10.1016/j.scitotenv.2016.06.135.
Vidal, C.B., Barros, A.L., Moura, C.P., de Lima, A.C., Dias, F.S., Vasconcellos, L.C., Fechine, P.B., Nascimento, R.F., 2011. Adsorption of polycyclic aromatic hydrocarbons from aqueous solutions by modified periodic mesoporous organosilica. J. Colloid Interface Sci. 357, 466–473. https://doi.org/10.1016/j.jcis.2011.02.013.
Wang, B., Gao, B., Zimmerman, A.R., Lee, X., 2018a. Impregnation of multiwall carbon nanotubes in alginate beads dramatically enhances their adsorptive ability to aqueous methylene blue. Chem. Eng. Res. Des. 133, 235–242. https://doi.org/10.1016/j.cherd.2018.03.026.
Wang, B., Lian, G., Lee, X., Gao, B., Li, L., Liu, T., Zhang, X., Zheng, Y., 2019a. Phosphogypsum as a novel modifier for distillers grains biochar removal of phosphate from water. Chemosphere 238, 124684. https://doi.org/10.1016/j.chemosphere.2019.124684.
Wang, B., Wan, Y., Zheng, Y., Lee, X., Liu, T., Yu, Z., Huang, J., Ok, Y.S., Chen, J., Gao, B., 2018b. Alginate-based composites for environmental applications: a critical review. Crit. Rev. Environ. Sci. Technol. 49, 318–356. https://doi.org/10.1080/10643389.2018.1547621.
Wang, J., Chen, Z., Chen, B., 2014. Adsorption of polycyclic aromatic hydrocarbons by graphene and graphene oxide nanosheets. Environ. Sci. Technol. 48, 4817–4825. https://doi.org/10.1021/es405227u.
Wang, J., Liu, X., Liu, G., Zhang, Z., Wu, H., Cui, B., Bai, J., Zhang, W., 2019b. Size effect of polystyrene microplastics on sorption of phenanthrene and nitrobenzene. Ecotoxicol. Environ. Saf. 173, 331–338. https://doi.org/10.1016/j.ecoenv.2019.02.037.
Wang, M., Hearon, S.E., Johnson, N.M., Phillips, T.D., 2019c. Development of broad-acting clays for the tight adsorption of benzo[a]pyrene and aldicarb. Appl. Clay Sci. 168, 196–202. https://doi.org/10.1016/j.clay.2018.11.010.
Xu, X.H., Hu, H., Kearney, G.D., Kan, H.D., Sheps, D.S., 2013. Studying the effects of polycyclic aromatic hydrocarbons on peripheral arterial disease in the United States. Sci. Total Environ. 461, 341–347. https://doi.org/10.1016/j.scitotenv.2013.04.089.
Yang, K., Yang, J., Jiang, Y., Wu, W., Lin, D., 2016. Correlations and adsorption mechanisms of aromatic compounds on a high heat temperature treated bamboo biochar. Environ. Pollut. 210, 57–64. https://doi.org/10.1016/j.envpol.2015.12.004.
Yang, Q., Gao, M., Zang, W., 2017. Comparative study of 2,4,6-trichlorophenol adsorption by montmorillonites functionalized with surfactants differing in the number of head group and alkyl chain. Colloid. Surface. Physicochem. Eng. Aspect. 520, 805–816. https://doi.org/10.1016/j.colsurfa.2017.02.057.
Zhang, C., Wu, L., Cai, D., Zhang, C., Wang, N., Zhang, J., Wu, Z., 2013. Adsorption of Polycyclic aromatic hydrocarbons (fluoranthene and anthracenemethanol) by functional graphene oxide and removal by pH and temperature-sensitive coagulation. ACS Appl. Mater. Interfaces 5 (11), 4783–4790. https://doi.org/10.1021/am4002666.
Zhang, L., Zhang, B., Wu, T., Sun, D., Li, Y., 2015. Adsorption behavior and mechanism of chlorophenols onto organoclays in aqueous solution. Colloid. Surface. Physicochem. Eng. Aspect. 484, 118–129. https://doi.org/10.1016/j.colsurfa.2015.07.055.
Zhao, S., Huang, G., Wei, J., An, C., Zhang, P., 2015. Phenanthrene sorption on palygorskite modified with gemini surfactants: insights from modeling studies and effects of aqueous solution chemistry. Water, Air, Soil Pollut. 227, 17. https://doi.org/10.1007/s11270-015-2716-8.
Zhu, L., Ren, X., Yu, S., 1998. Use of cetyletrimethylamonium bromide-bentonite to remove organic contaminants of varying polar character from water. Environ. Sci. Technol. 32 (21), 3374–3378. https://doi.org/10.1021/es980353m.